Investigating the Role of Calcium and Phosphocholine in αB Crystallin Oligomerization

Alexander Y. Dreisbach

Submitted to the Department of Biochemistry & Biophysics of Amherst College in partial fulfillment of the requirements for the degree of Bachelor of Arts with honors.

Advisor: Professor Patricia B. O'Hara

Readers: Professor William A. Loinaz,
Professor Patrick L. Williamson

4/14/17

Abstract

αB crystallin is a small heat shock protein, and functions as a molecular chaperone, preventing the aggregation of denatured proteins. One particularly interesting feature of αB crystallin is its ability to dynamically exchange functional homodimers to form polydisperse oligomeric species. This feature is believed to be of central importance in its function. Circumstances under which this feature is modified or inhibited are thus of great importance in gaining a better understanding of this function. Calcium(II), a common intracellular constituent and known player in many different cellular processes, has been identified as a good candidate for such modification. Similarly, phosphocholine, a motif of plasma membrane phospholipid headgroups within the eye lens, has been identified as a potential source of oligomeric modification. In this work we use Förster resonance energy transfer to interrogate the abundance and distribution of oligomers in the presence of the aforementioned small molecules. We find that both of these molecules induce little or no change in the oligomeric distribution of αB crystallin.

Acknowledgments

I owe an eternal debt to Professor O'Hara. Not only for her extensive knowledge and guidance in advising this work, but for bearing with me in my ineptitude and all-too-often forgetfulness.

Thank you to my readers, Professors William Loinaz and Patrick Williamson. I see it as fitting that you should be reading this, having collectively taught me the majority of what I know about biochemistry & biophysics.

Thank you to my friends, family, and teammates; for both encouraging me to pursue this, and for bearing with me during its completion.

Thank you to the many previous students of the O'Hara lab, without whose work I could not have done this. Thank you to Professor Hebda and the students of his lab, for graciously agreeing to supply purified αBC for assay.

And lastly, to Audrey, whose sage stature bore the brunt of many frustrating tales of lab work; you're alright, I guess.

Table of Contents

Table of Figures

Figure — Page Number

I . Introduction

Alpha-B crystallin (αBC), the most abundant protein in the lens of the eye, undergoes spontaneous and heterogeneous self-assembly in a manner which is not yet fully understood. In order to better understand this process, we employ the technique of FRET to measure the relative frequencies of αBC's different conformations in this region. To do this, fluorescent donor and acceptor dye molecules will be attached to monomers of αBC and their energy transfer will be used as a marker of dynamic oligomerization using Förster Resonance Energy Transfer (FRET).

A. Protein Folding and Molecular Chaperones

i. The Process of Folding

In the 1960s, Christian Anfinsen postulated that most proteins, in particular small proteins, contained all the information necessary to determine their final quaternary structure, within their primary sequence [1]. Further, he stated that these proteins will naturally achieve their native structure independent of additional support such as enzymes or ATP hydrolysis, should it be kinetically accessible, stable, and unchallenged in lowest free energy [1]. In a chaotic cellular environment, proteins independently achieving their functional state is crucial in proteome maintenance and cellular function in general. Protein folding is primarily driven by hydrophobic residues collapsing in on themselves, away from the aqueous cellular environment, to form a molten globule. Polar interactions among other amino acids contribute to the protein's secondary structure, forming characteristic alpha helices and beta sheets. Under normal conditions, most proteins fold into their native conformation on the order of milliseconds, with some proteins clocking at just a few microseconds [2]. However, a growing body of work in the wake of Anfinsen as modeled in Figure 1.1 suggests that not all proteins follow this model, and that some proteins must make use of other cellular resources to achieve their active form [3].

ii. Molecular Chaperones

A molecular chaperone is a protein which helps another protein to fold properly, but is not in any way bound to the assisted protein following completion of its task. Categorically, molecular chaperones are a rich and diverse group of macromolecules,

who collectively perform a wide variety of functions, including the maintenance of a cell's proteome .

After a protein successfully folds into its native conformation, there are a number of factors which could potentially make it less stable, including solvent constitution, post-translational modifications, assimilation into a larger complex, temperature, oxidation, aggregation, etc. Should a protein undergo a mis-folding event, there is the possibility that a hydrophobic area of the protein could be exposed, which could interact with other exposed hydrophobic surfaces to disrupt the cell's function

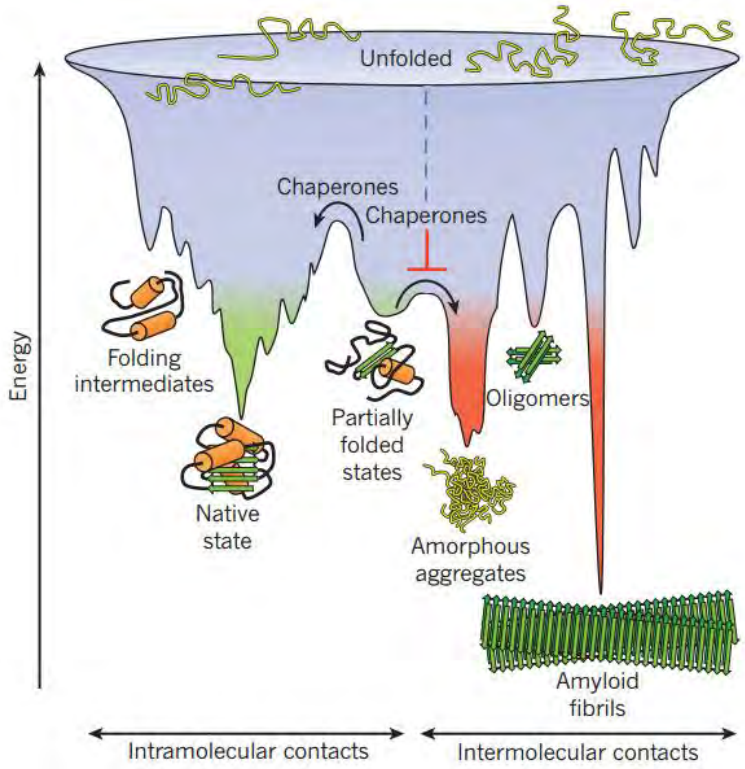

Figure 1.1: Energy landscape of protein folding. Chaperone proteins serve to bias energy minimization in favor of the native conformation of a protein. Adapted from ref. [4]

through protein aggregation or other adverse conditions. Chaperone proteins provide molecular chambers in which proteins can be kept apart from other interfering cellular components and allowed to fold in a safe and unobstructed environment.

Molecular chaperones were not initially discovered from this functional direction; rather, it came as a consequence of their study as Heat Shock Proteins (HSPs). Around the time that Anfinsen was performing his experiments on protein folding, Ferruccio Ritossa was studying the effect of unexpected heat shock on the chromosomal content of *Drosophila melanogaster*, fruit flies. He noticed a 'puffing' within the chromosomes when they were exposed to a rise in temperature [5], which Alfred Tissieres deduced resulted from a rapid up-regulation of mRNA production and subsequent protein production at the site of the puffing [6]. Thus these proteins, yet to be classified, were initially called HSPs.

In the 1970s, one particular heat shock protein, HSP60, also known as GroEL, was identified as being crucial in the formation of a lambda bacteriophage's head capsule [7,8]. In combination with GroES, it was one of the first proteins found to constitute a capsule-like structure, inside of which a protein could fold free from other cytosolic pressures [9]. In parallel with other discoveries regarding the wide range of functionalities in other HSPs, this discovery opened the door for HSPs to be studied as molecular chaperones, and myriad studies have been performed to show how closely tied HSPs are to molecular chaperone function [10].

iii. Protein Misfolding Pathology

The categorical failure of a protein to fold does not always remain a microscopic or cellular issue. Instead, it can present macroscopically. Indeed, a broad range of

human diseases arise from the failure of a specific peptide or protein to either initially find or remain stable in its native conformation. These include a number of well-researched diseases such as Alzheimer's Disease and ALS as well as less documented disorders [11]. The vast majority of these diseases are characterized by the formation of organized fibrillar structures through aggregation of their misfolded constituents. These fibrils accumulate in the target organ or organ system and consequently adversely affect normal biological function [11].

Affected tissues have multiple means of fighting these misfolding pathologies, not least among them the expression of molecular chaperones. αBC's successful chaperoning of various amyloid substrates has implicated it as a player in several of these diseases, including Alzheimer's disease [12,13] and multiple sclerosis [14].

B . Alpha Crystallin

i . Biological function

αBC was first discovered to function as a molecular chaperone preventing protein aggregation in the eye lens [15], to be discussed in greater detail in the following section. The list of αBC--and more generally small Heat Shock Protein (sHSP)--target proteins has since grown; recent studies have identified that sHSPs can successfully prevent the aggregation of approximately one-third of all cytosolic proteins [16]. From this, it makes sense that small heat shock proteins including αBC have been found to generally interact non-specifically; recently, structural dynamics studies employing NMR have reported that αBC utilizes both the highly flexible N-terminal region and the largely stable alpha crystallin core domain to capture different types of mis-folded proteins based on the target's conformation and flexibility [17]. This is supported by

research reflecting that chaperone function depends more on mass ratio than molar ratio [18], suggesting that the mechanism of sHSP's chaperone function relies on contact with a hydrophobic surface area rather than a specific sequence on a given target protein.

However, simply covering exposed hydrophobic surfaces in general does not adequately describe the mechanism of sHSPs. First, a proper degree of selectivity must be maintained in order to alleviate stress on cellular proteostasis pathways. An overly selective sHSP would be inefficient, while a completely non-specific sHSP could interact with stable, native proteins and otherwise interfere with a cell's proteome [19]. In addition, the sHSP must exhibit great enough binding affinity to out-compete other exposed hydrophobic surfaces in order to effectively prevent aggregation. While it has been shown that αBC does interact with some native proteins [20], and can also de-aggregate in some cases [21], it is generally the case that αBC interacts with proteins which maintain most of their core structure or a significant fraction of their native secondary interactions while exposing a hydrophobic target surface [21,22].

Second, once the sHSP has formed a complex with a target, it must effectively determine the fate of the protein. Small heat shock proteins perform a 'hold-ase' function, where the sHSP stabilizes the target protein through an ATP-independent action, in a conformation which allows it to be re-folded through another mechanism [23] as shown in figure 1.2. Although the sHSP does not perform this task itself, it can interact with certain ATP-dependent mechanisms to facilitate this re-folding [23]. Alternatively, the sHSP can interact with components of the ubiquitin proteolytic pathway to direct substrates toward degradation [24,25].

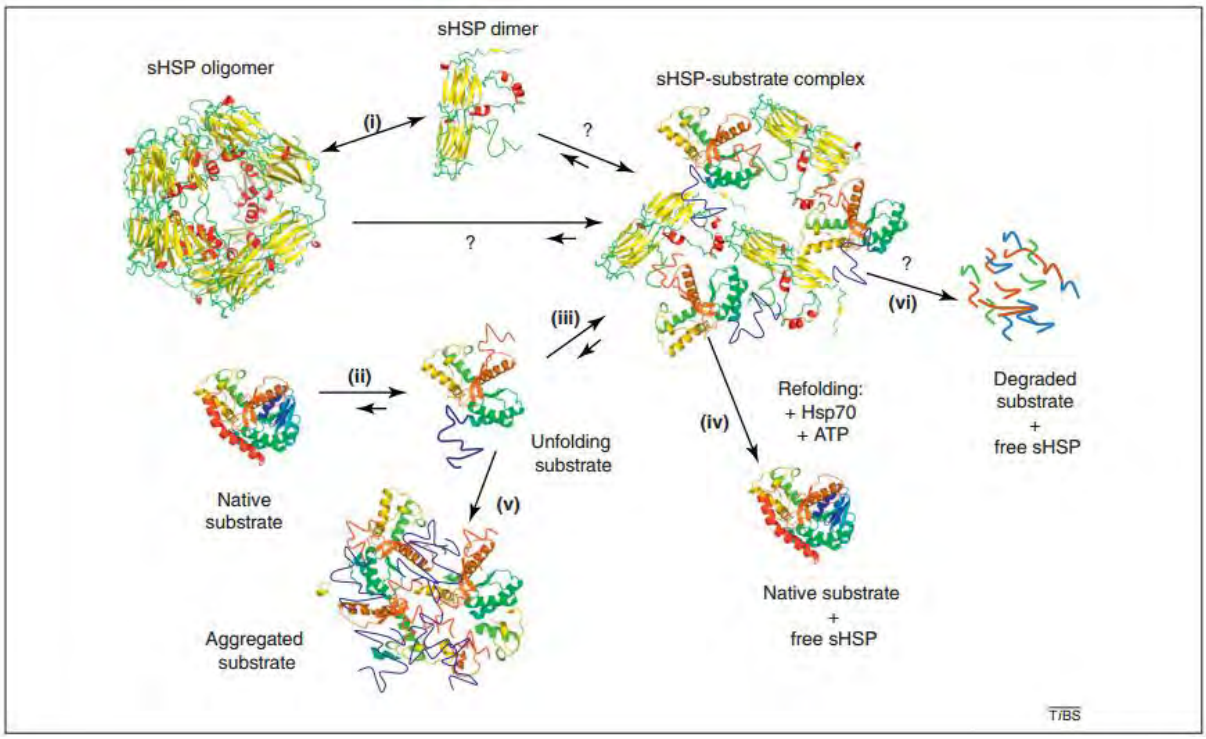

Figure 1.2: A model for sHSP chaperone function. sHSPs can complex with mis-folded proteins to direct them towards refolding or degradation in multiple ways. Adapted from ref. [18]

Other functions for αBC have been reported beyond aggregate prevention. Research has shown that αBC plays an important role in regulating the dynamic polymerization of actin [26,27], as well as being involved in the stability of microtubules [28,29] and intermediate filaments [30]. Because of these findings, in combination with αBC's expression in brain tissue, defective αBC has been implicated in neurodegenerative diseases such as Alzheimer's disease [12] and multiple sclerosis [14]. Furthermore, it can be implicated as factor in any number of pathologies relating to protein aggregates.

αBC has been shown to be subject to a number of post-translational modifications, which present varying degrees of influence on chaperone activity [31,32]. These modifications allow for αBC to be better suited to particular environments as it is

differentially expressed within a system, for instance adapting it to the differing environments of the eye lens and brain tissue. In particular, three phosphorylation sites have been identified on the N-terminal domain of αBC [33]. Studies show that phosphorylation of these sites changes chaperone function to varying degrees [34]. In conjunction, phosphorylation has been shown to affect the oligomerization behavior of αBC [34].

ii. Alpha B Crystallin in the eye lens

A perfect example of the connection between protein stability and noticeable pathology is the eye lens. The lens' function is to focus incoming light received through the cornea and project it onto the back of the eye at the retina, as is shown in Figure 1.3.

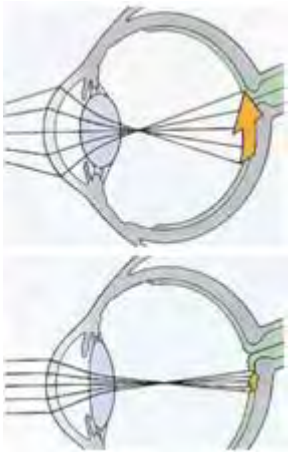

Figure 1.3: Eye lens functionality.
http://www.visionaware.org/info/your-eye-condition/eye-health/anatomy-of-the-eye/125

In order to be successful, the optical path must naturally be clear, and as a consequence the optical path in the eye must be transparent. Any structure within the lens that has approximately the wavelength of the transmitted light has the potential to scatter light and disrupt the image. A sufficient concentration of these structures will severely

hinder vision, and is observed as cataracts. Alpha crystallins serve to protect against the formation of these structures as a molecular chaperone within the lens [15].

What complicates the eye lens compared to other parts of the body is the lack of proteostatic cellular machinery. This makes sense -- organelles such as mitochondria, nuclei, ribosomes, lysosomes, and endoplasmic reticulum are all large enough to scatter light and must be removed from the optical path. This happens during the maturation of fiber cells within the lens. With no way of exchanging materials with the external environment, the lens must stay transparent over the human lifetime of approximately 100 years, far longer than most other proteomes within other types of tissues, which (depending on the protein) can turnover protein on a scale of hours to days [35]. Furthermore, with no energy-dependent mechanism to offload mis-folded substrate onto, αBC has a finite capacity to perform its function before it is overwhelmed and aggregates may form. This process can speed up in the presence of any number of factors including charge inversion and ion concentration changes, but particularly in terms of the previously discussed post-translational modifications which alter αBC function [34].

αBC is not alone, however. There exists another iso-form of alpha crystallin, alpha A, which shares 57% sequence homology with αBC. Their differences primarily lay in their N- and C-terminal extensions. They work alongside β- and γ-crystallins, which serve a similar purpose of molecular chaperoning, although their target proteins vary slightly.

The significance of alpha crystallin in preventing cataracts was reported by knockout studies in mice [36]. Notably, alpha-A knockout mice suffered cataracts quickly,

however alpha-B knockout mice did not [37], suggesting either a different role of alpha-B within the lens or differing functional load between the two isoforms.

With regard to its function, αBC in the lens functions much in the same way as elsewhere in the body in its molecular chaperone functionality, but also plays a structural part. Alpha crystallin by itself makes up about 40% of the protein within the lens at concentration of approximately 400mg/mL [38]. Together with β- and γ-crystallin, these three protein families make up approximately 90% of the protein within the lens [39]. These different proteins are differentially expressed along the direction of the optical path within the eye to correct for spherical aberration [40]. With these proteins being so tightly packed, it is crucial that they each be able to avoid crystallization or aggregation, lest they compromise their own function. This is why the heterogeneous formulation of αBC oligomers is so crucial in order to counteract any sort of repetition among small oligomers, which could form a crystal structure.

iii. Structure and Oligomerization

Alpha crystallins, as members of the small heat shock protein family, inherit certain common characteristics which give us a broad understanding of αBC, namely: a small molecular mass of about 12-43kDa, the ability to self-assemble into dynamic, polydisperse oligomers (to be discussed later in this chapter), a conserved alpha crystallin core domain, and their function of preventing protein aggregation [4].

The most recognizable feature of αBC is its core domain. This sequence contains an average of 94 residues across sHSPs, making it the primary structural constituent of these proteins, who average a total length of 161 residues [41]. As previously stated, this core domain is conserved across the sHSP family [42], although the primary sequence of

this domain is not. Rather, it is characterized by its tertiary structure of two approximately plane-parallel beta-sheets, which bears resemblance to immunoglobulin's core domain. In αBC, the core domain comprises approximately 85 of its 175 amino acid constitution.

On one side of this core is the C-terminal domain. αBC has a C-terminal domain of 25 residues, significantly greater than the average length of 10 residues across all sHSPs. On the other side of the core domain is the N-terminal domain, whose 56 residue length is much closer to the sHSP family average of approximately 60 residues. Although both the N- and C-terminal domains have been shown to contain significant secondary structure [43], there is little evidence to suggest that these domains play a significant structural role and are considered to be largely disordered. However, they each have been implicated to serve roles in the oligomerization of αBC.

Oligomerization plays a crucial role in understanding the action of sHSPs as molecular chaperones, as alluded to in previous sections. The dynamic self-assembly of larger multimers and dispersion into smaller units (the latter of which are generally thought to be the functional form of αBC) which results in a polydisperse distribution of oligomers, is both a well-known and not-well-understood process. An important part of understanding oligomerization is understanding how the substructures of alpha crystallin contribute to the process. Unfortunately, the same flexibility in the N- and C-terminal domains which have been reported as important in chaperone function and are crucial in preventing crystallization within the eye lens (and will later be discussed regarding their proposed role in oligomerization) prevent alpha crystallins from forming a regular, ordered crystal structure which would allow it to be studied by

conventional crystallography techniques [44]. Thus, a structural analysis of oligomers themselves, the most direct route to a better understanding of oligomerization, is consequently impeded. However, NMR spectroscopy and X-ray crystallography structures have recently been reported for the αBC core domain lacking both N- and C-termini, such as 2KLR [45,46].

Within the core domain there exists a binding interface along the beta-7 strand, and the anti-parallel binding of two of these strands forms the functional dimeric iterance of αBC, the homo-dimer. As a result, the constitutive beta-sandwiches are conjoined along the edge of the sheets laterally to form a wider sandwich and not stacked vertically as shown in Figure 1.4.

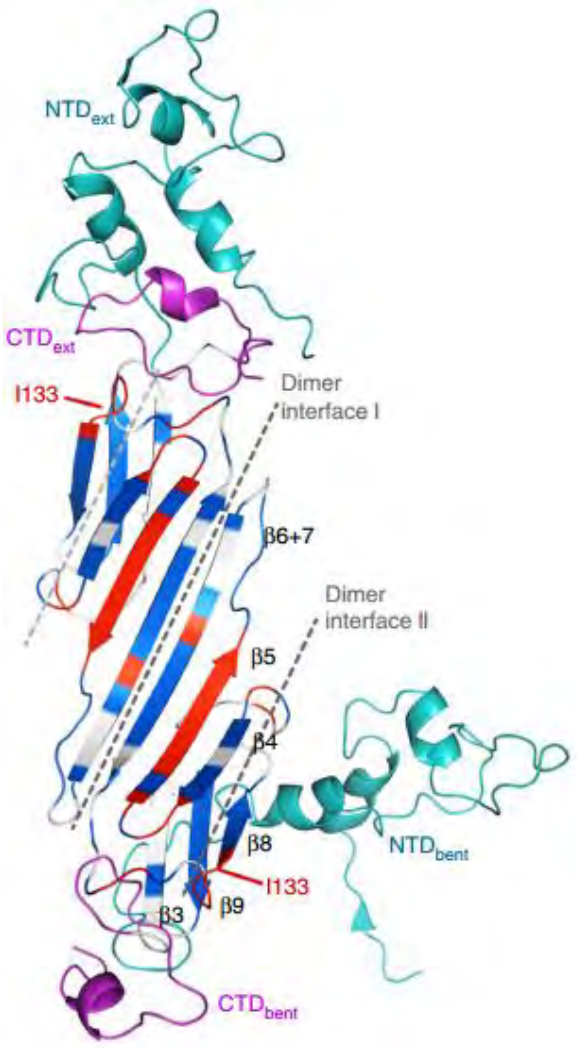

Figure 1.4: The functional unit of αBC. Dimer interface I illustrates the lateral conjoining of beta sheets, while Dimer interface II illustrates C-terminal binding into the beta-4/beta-8 groove. Adapted from ref. [17].

Both the N- and C-termini appear to have a role in the dynamic self-assembly of αBC into higher-order oligomers. The C terminus contains an isoleucine-X-isoleucine motif which has been observed to bind in the beta-4/beta-8 pocket within the core domain of another monomer, both intra-dimer and between dimers, as a form of domain swapping to mediate oligomer formation [47]. The palindromic nature of this sequence is postulated to contribute greatly to the polydispersity of αBC by allowing equally favorable binding interactions in both orientations [48]. Further, mutations in the C-terminal domain of αBC lead to abnormal chaperone function and oligomerization, and are linked to certain diseases [13]. The N-terminal domain has also been incorporated into the discussion surrounding oligomerization. Although it has been shown to contain significant secondary structure, the N-terminal domain lacks specific sequences which has been previously shown to facilitate binding [49], complicating predictions surrounding its role in oligomerization. However, it has been observed that deletion of the N-terminal domain causes αBC to not be able to form oligomers [50], giving strong evidence that it does participate in one way or another. In addition, studies have shown that there exists at least one sequence within the N-terminal domain which participates in subunit-subunit interactions [51].

αBC oligomeric size distribution is an approximately a Poisson distribution centered around a 28 monomer oligomer, or 28mer, when the fit is constrained to oligomer sizes of 10mer to 50mer [52]. In addition to self-assembly, alpha crystallin can participate in the assembly of hetero-oligomers, oligomers formed out of multiple kinds of small heat shock proteins which have been observed to co-assemble, furthering αBC's polydispersity [53]. αBC oligomers undergo changes in state with a subunit

exchange rate on the order of 10^{-4}/second at 37°C, corresponding to complete mixing of oligomers over a period of four hours [54]. Models of αBC oligomers generally tend to agree that there is relatively little structural difference in environment between functional dimers within an oligomer [54]. This helps to explain both the polydispersity of αBC oligomers through equally energetically favorable binding interactions, which reduces the bias in oligomer size, and the high rate of subunit exchange, through low binding preference.

Recently, theoretical structural models have been put forth to explain αBC polydispersity which describe αBC oligomerization as hierarchical: three homo-dimers assemble into a hexamer, mediated by inter-dimer C-terminal domain swapping into the beta-4/beta-8 groove; these hexamers are arranged into larger, more spherical oligomers by means of N-terminal interactions which are not yet fully understood [55]. Oligomers in this model appear to have a 24mer bias (as represented in 3J07), with binding surfaces as pockets on the surface or on the inside of the oligomer 'shell' providing a means for the formation of differently sized constructs. In support of this model, studies have shown that disruption of the N-terminal domain by means of incorporating negative charge through either phosphorylation or altering the N-terminus' primary sequence results in an oligomeric size distribution shift toward smaller oligomers and a dramatic increase in oligomers existing in multiples of six monomers [55,56]. Further, these experiments show an increase in chaperone activity.

The relationship between oligomerization and αBC's chaperone function is less well understood than oligomerization's relationship with structure. As previously mentioned, hydrophobic substrate binding sites have been identified in each of the

three main sections of αBC, all three of which also participate in the protein's oligomerization. A competition between the use of αBC's hydrophobic sequences is thus postulated to be the link between oligomerization and function, leading to a model which purports that oligomers serve as 'storage areas' for αBC, whose disassembly into smaller oligomeric or dimeric forms allow it to perform its chaperone function [57]. This idea is complicated by the fact that αBC can prevent aggregation on a timescale faster than that of subunit exchange, leading to the fact that the oligomeric form must in some way be able to perform the chaperone function [54]. Nonetheless, it appears that oligomerization and function of αBC are dynamically linked by the competition for hydrophobic sequences.

iv. Calcium and Phosphocholine's Role

Calcium is well known to be a powerful intracellular tool. Whether it be cell signaling, enzymatic regulation, or cell motility, calcium is known to have a profound effect on cells. This also includes deleterious effects like protein misfolding and calcium-induced aggregation [58]. It is no surprise, then, that calcium levels are tightly regulated in most cellular conditions. Within the context of the eye lens, the plasma membrane calcium ATP-ase (PMCA) and the sodium/calcium exchange membrane protein (SCEP), alongside the varying and small passive permeability of the plasma membrane to calcium determine its levels within mature nuclear fiber cells [59]. Cortical cells of the lens, which retain greater amounts of cellular machinery during cell differentiation, have a more robust network for calcium regulation than these cells [58]. In healthy lenses, these cells have a slightly elevated calcium concentration with respect to nuclear cells [58]. However, in cortical cataractous lenses, cortical cells have significantly higher

calcium concentration than nuclear fiber cells (which retain relatively normal levels of calcium), providing evidence for theories of differentiable cataractogenesis. αBC is generally not invoked in explanations of cortical cataractogenesis, however this does not mean it is not important. Previous studies have shown αBC can aggregate under sufficient calcium concentrations [60]. However, other studies show that cellular pH levels can be too high for this too occur [61]. A further understanding of how calcium modulates the quaternary structure and function of αBC is important in developing models of cataractogenesis and subsequent sHSP modulation.

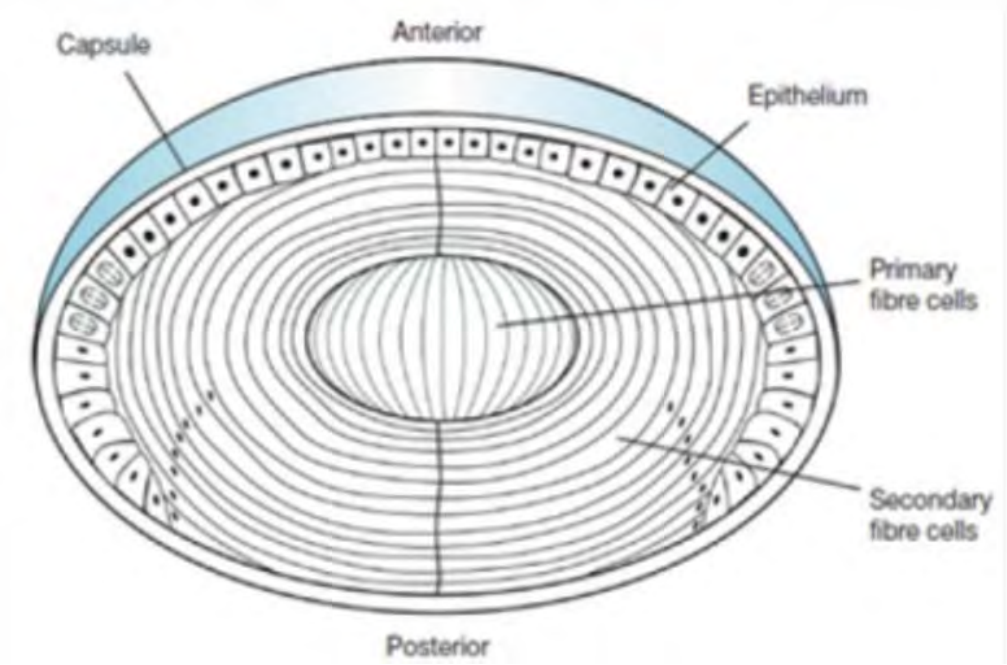

Figure 1.5: Cellular structure of the eye lens. Primary fiber cells are within the nuclear region, while secondary fiber cells make up the surrounding cortical region. Adapted from ref. [62]

Within the nuclear portion of lens, shown as the primary fiber cells in Figure 1.5, plasma membrane lipid constituency is a dynamic metric. It contains an unusual amount of saturated fatty acid chains, alongside an unusually high cholesterol level in

comparison with other areas of the body [59]. Lens lipids evolve over time, and are subject to aging and are affected by numerous pathologies. As we have previously seen, they are important in maintaining ion levels, although their permeability increases with age. In fact, it is estimated that the outer leaflet of nuclear lens cells contains enough phospholipid character to sequester all of the extracellular calcium [59].

αBC's relationship to nuclear cell membrane lipids is complicated. In recent years, it has been shown that αBC binds to the plasma membrane, and that the frequency of this binding increases with age and cataract formation [63]. However, the mechanism of this affinity has not been subject to much scrutiny, and so the question remains as to how this is accomplished. One possibility is that αBC binds to transiently exposed hydrophobic tails of these lipids, as though they are long denatured proteins to chaperone. Another possibility is that αBC increases in its affinity for the charged headgroup species present in these lipids, particularly phospholipids, given that it is known αBC's activity and structural dynamics are altered when it is phosphorylated. The major players in the nuclear cell membranes are sphingomyelin and phosphotidylcholine. Both of these lipids contain a functional group called phosphocholine (hereafter referred to as PC, *not to be confused with phosphotidylcholine*): a phosphate group linked to a trimethyl quaternary amine by two saturated carbons, as illustrated in Figure 1.6. As a zwitterionic constituent, it is a good candidate to initially test αBC's affinity for charged lipid headgroups, even when free in solution. Understanding αBC's changing membrane affinity could be key both in understanding its function and how it could be prevented from sequestering itself.

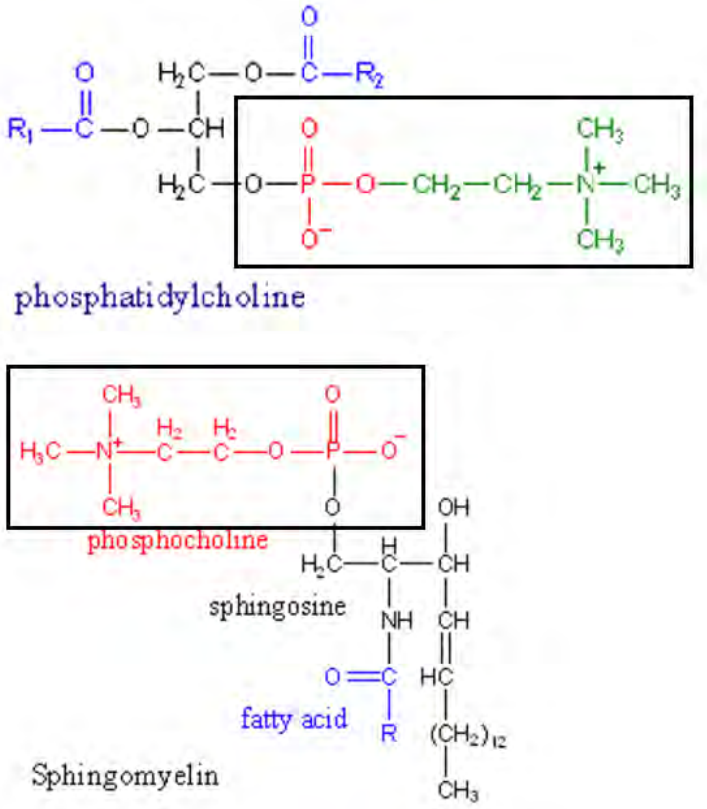

Figure 1.6: Molecular structure of phosphotidylcholine and sphingomyelin. Each contains the phosphocholine motif outlined with a black box. Adapted from ref. [64]

v. My questions

In this work we seek to provide a qualitative analysis of calcium- and PC-induced modulation of αBC oligomerization and structure. With regard to PC, it is unlikely that it significantly affects the structural dynamics of αBC, if at all--αBC has relatively low affinity for charged species, therefore it is likely a non-factor. Nonetheless, an unchanged oligomeric distribution would provide evidence for the elimination of lipid headgroups as the source of αBC's membrane affinity. Calcium shows more promise, if only for its history. Modification of αBC's oligomeric distribution by calcium could provide insight as to how αBC contributes to cortical

cataractogenesis, and how αBC could be inhibited or otherwise changed. In total, observing how relevant small molecules affect αBC oligomerization could help improve cataractogenesis models and expand our knowledge of sHSP structure and function. Single-molecule FRET is a good candidate for investigating this change, as it can detect shifts in oligomeric subpopulations even if the average state of αBC is relatively unchanged.

C. Fluorescence

Since the introduction of fluorescence as a tool in probing biological systems, fluorescent spectroscopy has grown to be one of the most popular methods of investigation and measurement within the field. In considering our method of investigation, Förster Resonance Energy Transfer (FRET), it is best to first understand the general principles of fluorescence before considering how FRET utilizes them.

i. Absorption and Emission

There are two general causes of light emission, classified according to the means by which the molecule was excited: incandescence, which refers to molecules excited through thermal means; and luminescence, which encompasses all other means of excitation. The process of fluorescence falls within the latter of these two categories. Fluorescence is a photo-luminescent process, which means that the molecule being observed was excited by a photon.

Photo-luminescence is a process which involves molecules (fluorescent molecules are generally called fluorophores) transitioning between quantized electronic energy levels. At STP, fluorophores exist in their ground electronic state, and populate their lower vibrational states. Excitation of this fluorophore occurs when an

incident photon matches energy difference between the fluorophore's current ground state and one of the vibrational energetic states within an a more energetic electronic state as shown in Figure 1.7. From here, the fluorophore relaxes to the lowest vibrational energy level within the excited electronic state by way of thermal contact with the surrounding medium.

Molecules in the lowest energy excited electronic state can vary with respect to their stability. Factors contributing to this will be discussed in greater detail in section I.B.iv. Generally, molecules in this state are significantly more stable than those in higher vibrational states, due to the large energy difference between electronic states relative to vibrational states. As such, fluorescent emission usually occurs from this state. Emission is the release of a photon by the molecule equal in energy to the difference between the excited state and one of the vibrational energy levels within the ground state. Absorption and emission together constitute a fluorescence event.

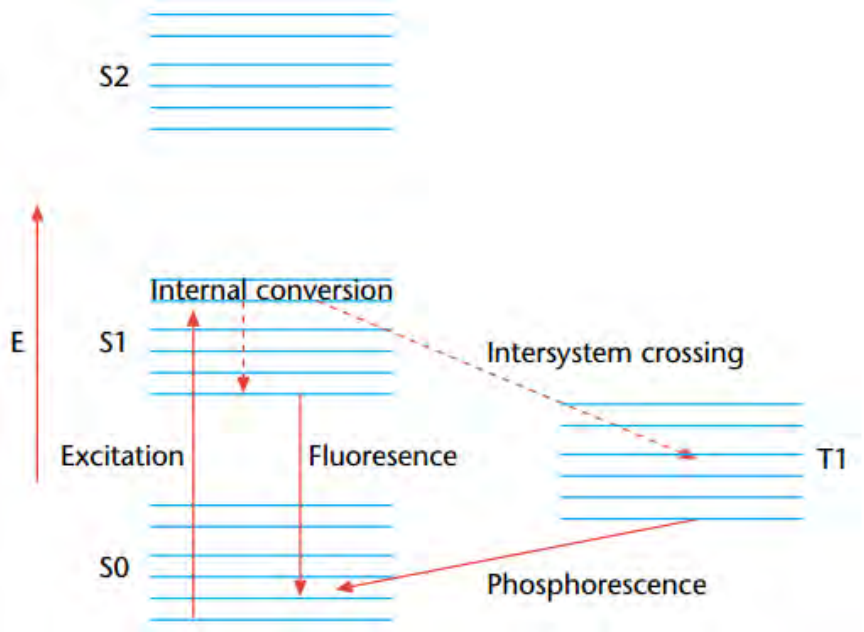

Figure 1.7: Energy level diagram of fluorescence. Adapted from ref. [65]

Fluorophores are largely characterized by their absorption and emission spectra, which describe the relative frequency of the absorption or emission event with respect to the relevant wavelength of light. On the basis of the prior explanation of absorption and emission alone, one might believe that these spectra are defined by sharp peaks corresponding to wavelengths whose photon matches a vibrational and electronic energy level difference within the fluorophore. In reality, fluorophore interactions with the solvent broaden these peaks to give these spectra their characteristic curves. Similarly, one could intuit that because absorption and emission are symmetric events, in the sense that they corresponding to transitions between the same energy levels, that absorption and emission spectra should completely overlap. In reality, the thermal relaxation of an excited molecule to its lowest electronically excited state causes the emitted photon to be crossing an energy difference slightly less than that of the excitation photon, and as a result the emission photon is redshifted. As this happens to varying degrees across all wavelengths, emission spectra are characteristically redshifted with respect to absorption spectra, called the Stokes shift.

ii. Radiative and non-radiative means of relaxation

Beyond exiting the excited state through emission of a photon, a molecule can relax through a number of non-radiative means. The overwhelming majority of non-radiative relaxation of an excited molecule is thermal. This happens when the lowest excited state of a molecule overlaps with one of the vibrational energy levels of the ground electronic state. The molecule undergoes internal conversion to occupy this vibrational state, from which it relaxes thermally to its ground vibrational and

electronic state. It can also de-excite through collision with the solvent and other materials in its proximity.

Non-radiative relaxation which is not thermal in nature is generally termed 'quenching.' Quenching usually involves an excited molecule-molecule interaction rather than interactions with the surrounding solution. Common means of quenching are collision with triplet molecules such as oxygen or a halogen, phosphorescence, or electron transfer. Another means of this quenching is FRET. In the following section, we consider the theory and mechanics of FRET, in order to give a better understanding of how to interpret its results.

iii. FRET

The process of FRET begins with a fluorophore in its excited electronic state, whose excitation in most experimental circumstances was stimulated by photon absorption. This fluorophore, denoted as the donor fluorophore, relaxes by means of energy transfer through electrodynamic coupling to another fluorophore, the acceptor fluorophore. Through this process, the acceptor fluorophore is electronically excited, and its relaxation is usually mediated by photon emission. Note that FRET itself does not necessitate use of any part of the fluorescent process, however fluorescent emission is generally used to quantify the states of the donor and acceptor because using fluorescent spectroscopy is generally the easiest way to record FRET in this context.

The means of energy transfer, naturally, is the novel part of this technique. The theory of FRET was developed by Theodore Förster, who published his work in 1948 as a quantitative analysis of his theory. It characterizes the excited donor as a Hertzian oscillating electric dipole. The corresponding dipole of the acceptor is then affected by

this oscillating electric field in the same way as it would interact with light as a source of electromagnetic radiation. If the dipoles are in suitable orientation relative to each other and the interaction is energetically favorable, energy is transferred from the donor to the acceptor via the electric field. The process can be represented in concept through the chemical equation

$$D^* + A \rightarrow D + A^* ,$$

where D denotes the donor fluorophore, A the acceptor, and * denotes the fluorophore in the excited state, and is represented in Jablonski form in Figure 1.8.

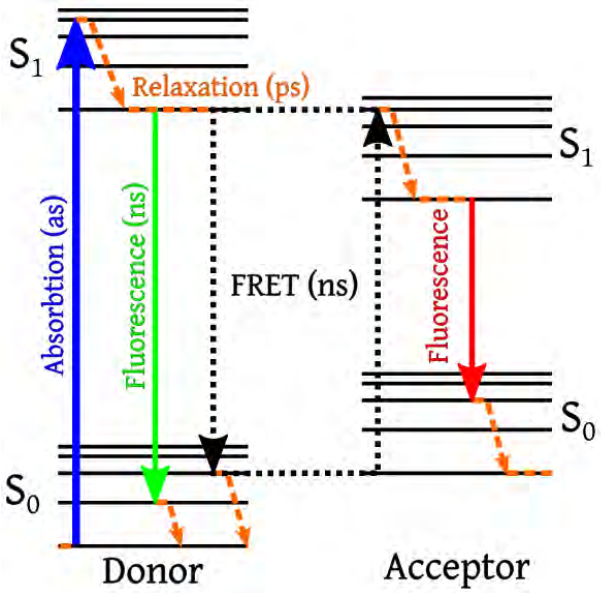

Figure 1.8: Jablonski diagram illustrating the process of FRET. https://commons.wikimedia.org/wiki/File:FRET_Jabolinski_Diagram.svg

iv. Dye selection

When implementing an experiment using FRET, selection of fluorophores is an important step. FRET is a process which requires a certain degree of compatibility, both between the fluorophores themselves as a donor and acceptor pair in a physical sense, and between the fluorophores and the rest of the system as a matter of practicality. In

the vast majority of FRET applications, a suitable pair is not found within the system of interest. As such, commercially available fluorescent dyes are usually affixed to the system at points of interest. From a procedural standpoint, the first requirement is thus to use dyes which can be uniquely attached to the system and purified.

With respect to being an efficient FRET pair, the donor fluorophore must have a quantum yield (which is a measure of how often de-excitation occurs through fluorescence) large enough that it can be relied on as a stable source of energy, greater than approximately .01. On the other side, the acceptor fluorophore must have a large enough absorbance coefficient, reflecting the need for the acceptor to reliably receive resonance energy from the donor. The fluorophore pair must be situated in a way which allows for free rotation in three dimensions, to account for the postulate within the theory of FRET stating that the dipole interaction is not spatially constrained to certain orientations.

In addition, there must be sufficient spectral overlap between the emission of the donor and the excitation of the acceptor as shown in Figure 1.9. Again, although FRET is a non-radiative process, and thus we are not concerned about the energy of an emitted or absorbed photon, the direct relationship between photon wavelength and energy of the source molecule's excited state lets us infer about how well any two fluorophores will work as a FRET donor and acceptor.

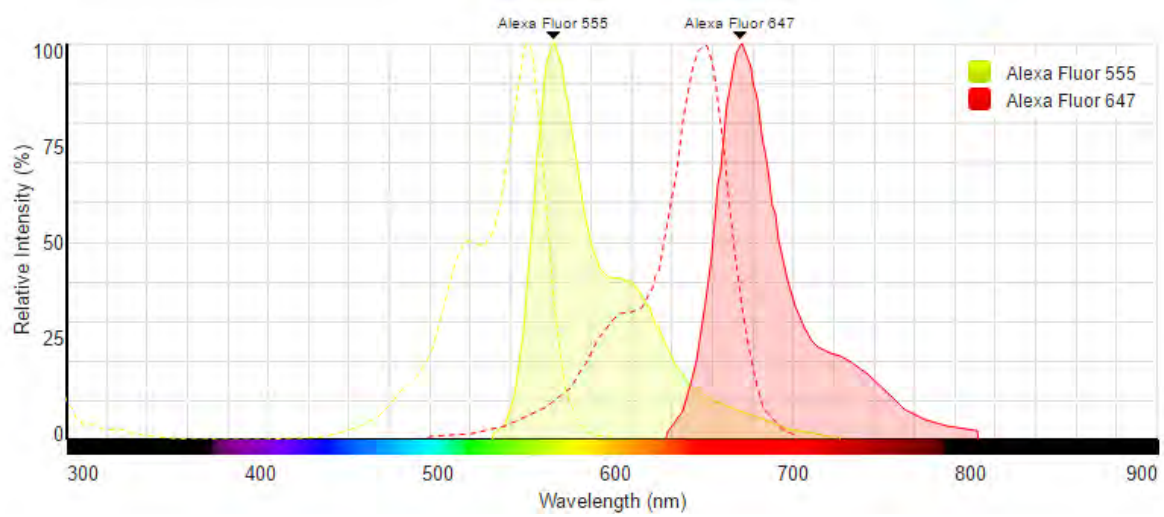

Figure 1.9: Spectral diagram illustrating the overlap of the two dyes used in this work. Note the vanishingly small excitation of AF647 at 532nm, and the presence of AF555 emission character at 650nm.
https://www.thermofisher.com/us/en/home/life-science/cell-analysis/labeling-chemistry/fluorescence-spectraviewer.html

Subject to the spectral properties of each fluorophore, the pair will have an effective range of about 10-100 Angstroms, in which they will be able to report on small changes in inter-dye distance. For any given pair, the distance at which FRET is 50% efficient is called the Förster distance. It is important to select a FRET pairing whose Förster distance is as close as possible to the distances one intends to measure. Because of FRET's efficiency relating to distance to the sixth power, FRET measurements outside a factor of two of the Förster distance are not reliable.

v. Single molecule FRET

Despite the fact that many chemical and biological systems are described by actions and structures on the molecular scale, most observational techniques utilize macroscopic measurements, and use extensive analysis and statistical modeling to infer the landscape of the system on a molecular scale. Single-molecule techniques are

advantageous in that they directly observe these characteristics rather than inferring them. Single molecule FRET observes the interaction of one donor and one acceptor to directly report on the state of one macromolecule. This is important, especially when considering a system whose sole constituent self assembles into polydisperse, heterogeneous conformations, such as alpha crystallin.

In bulk FRET, only the weighted average of the system's various states is reported based on the average intensities of donor and acceptor fluorescence over the observational volume. In single molecule FRET, individual molecules' fluorescence is quantized, and the tallying of these fluorescent quanta gives a FRET distribution that can report not only multiple distinct states, but the relative frequency of each state. Similarly, bulk FRET does not give a clear picture of dynamic processes that may be occurring over the time of observation, reporting only the general trend of the sample. In contrast, single molecule FRET can report on dynamic processes through differences in the FRET efficiency distribution and relative frequency of subpopulations. Extending this further, single molecule FRET can be used to detect rare divergences from a corresponding 'normal' distribution of states, which would otherwise be lost in bulk FRET.

The single molecule FRET implementation we used was designed to observe macromolecules freely diffusing through a liquid medium. In general terms, a laser tuned to excite the donor almost exclusively is focused on a small volume (small enough to house only one molecule of interest at a time) using a confocal microscopy set-up. Fluorescent emission from the molecule is captured by the same confocal objective, and is deflected through a series of dichroic mirrors to separate it into its donor and

acceptor portions. The intensity of light, as measured through number of photons received, from each of these channels is then used to calculate the efficiency of FRET for the molecule.

II. Materials and Methods

A. Experimental Components

αBC expression, purification, fluorescent labeling, and concentration determination was performed by the lab of Professor James Hebda at Austin College in Texas. Protein was received as separate stocks of donor- and acceptor- labeled protein in a sodium phosphate and sodium chloride buffer solution and stored at -80°C until ready for use. Protein to be used in the assays were stored at 4°C at micromolar quantities, before being diluted to nano- and pico-molar quantites with experimental buffer prior to assaying.

The 85th residue of αBC, a serine, was mutated to a cysteine in the DNA primary sequence prior to expression in *E. coli*. After αBC expression and purification, Alexa Fluor fluorescent dyes AF555 and AF647 were uniquely attached to this S85C residue (whose relative position and inter-dye distance is shown in Figure 2.1), given that this cysteine was the only cysteine residue in αBC's primary sequence. αBC-S85C reliably retained its chaperone function, as measured by the Hebda lab. αBC S85C is the only αBC mutant utilized in this work.

Figure 2.1: Position of S85C residue. Also shown is the inter-dye distance within a dimer.

Buffer solvents were assembled from their constitutive solutes available from Sigma Aldrich and HPLC water, pH balanced using aqueous sodium hydroxide and dilute hydrochloric acid.

B. Single Molecule FRET

i. The O'Hara Lab Single Molecule Apparatus

The primarily methodology for observing the FRET phenomenon in this work is through the single molecule detection system of the O'Hara Lab. In general terms, the system consists of laser excitation, confocal microscopy elements, and photodiode detection. The current iteration of the set-up contains a B&W Tek solid state monochromatic 532 nm laser, an Olympus IX71 inverted confocal microscope, and Perkin-Elmer SPCM-AQR avalanche photodiodes (APDs) in each of these respective places along the optical path. For recording data, a BNC-2121 card receives the output of the APDs, and connects it to a National Instruments PXI-6602 counter card within the lab computer to produce intelligible numerical photon counts quantized by bin. The system, in both its general and specific forms, was created by previous students of the O'Hara lab. Their work served as the primary information source for this section, and further contains a more detailed description of both the system's constituents and the reasoning behind their usage [66]. In addition, application of this system to interrogating αBC structural dynamics was accomplished by previous students of the O'Hara lab, and their methodologies provided a large basis for the procedures outlined in this work [67].

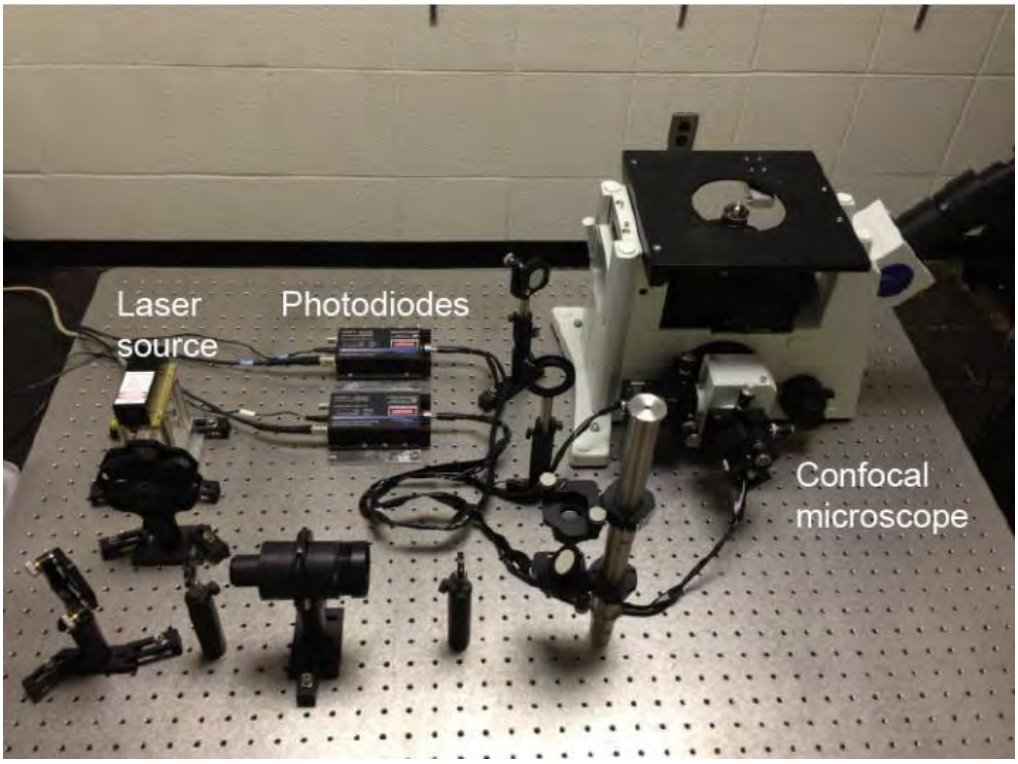

Figure 2.2: Table-top view of the O'Hara lab single-molecule FRET setup. Adapted from ref. [67]

Of the requirements for properly utilizing this system, operation in the single molecule domain is of the greatest importance. Knowledge of the system's optical path and focal volume in relation to the observational sample is therefore important as a method of ensuring acquired data to be attributed to the state of one donor-acceptor pair. In confocal microscopy, excitation photons are focused through a high numerical aperture objective onto a small volume. Photons resulting from the interaction of the excitation light and the dye pair are focused back through the same objective. To select for light from the focal plane out of all the light traversing back through the objective, a pinhole aperture is placed in the focal plane's corresponding image plane. This light from the focal plane is received by the signal detection mechanism. In our particular optical setup, laser excitation is sent through a 10x beam expander, before being

focused by the objective through the bottom of the sample. In the process of collection, the pinhole aperture selecting for light from the focal plane is adjoined to a fiber optical cable, coupling the APD to the microscope.

To calculate the focal volume, the volume can be approximated as a cylinder. It's radius is equal to the radius of the first-order diffraction-limited Airy disk formed by the objective in the focal plane, r: $r = .61\frac{\lambda}{NA}$, where λ is the wavelength of the excitation light, and NA is the numerical aperture of the lens. In our system, $\lambda = 532$nm and NA is 1.2, giving a radius of 270nm. The height of the cylinder can be approximated as the objective's depth of focus, D, where $D = 2\frac{\pi r^2}{\lambda}$. From our previous calculation of r, D is approximately 860nm. This gives an approximate focal volume of 0.20 fL. As a measure against loss of precision due to micro-scale variations in the optical path day-to-day, in addition to the focal volume not having a clear boundary, calculations regarding the focal volume used an approximation of 0.5 fL. Previous analysis using Poisson statistics has shown that for this focal volume, an αBC concentration of 3nM corresponds to one molecule in the volume at a given time, and that operation at concentrations lower than this threshold reasonably ensures that collected data can be attributed to single molecule dynamics.

Beyond ensuring that the apparatus operates in the single molecule domain, the next requirement of the system is proper segregation of light signals along the optical path. In this system, this is accomplished using a series of dichroic mirrors, as shown in Figure 2.3. Dichroic mirrors function by reflecting or transmitting light, based on one or more wavelength cutoffs, determined by the mirror's coating. These cutoffs can make

the mirror long-pass, short-pass, or band-pass, referring to the transmittance of those wavelengths that are either longer, shorter, or within the range of wavelengths specified by the coating. Laser light entering the microscope transverse to the objective first encounters a 550nm long-pass filter, meaning that the 532nm laser light will be reflected up toward the objective, while any stray light above 550nm will be transmitted and leave the optical path. This is one way to minimize erroneous data by preventing any direct excitation of the acceptor dye beyond 532nm light, which is of vanishingly small likelihood. After passing through the objective and into the focal plane, the light can interact with the FRET donor fluorophore, Alexa Fluor 555. Within the scope of this work, the excited dye can do two things: it can either fluoresce, or undergo FRET energy transfer to the acceptor dye, Alexa Fluor 647, which can then relax through fluorescence. The resultant light travelling back through the objective encounters a separate 550nm long-pass filter. Since donor fluorescence is Stokes shifted to above 550nm from 532nm excitation, and acceptor fluorescence must be of a greater wavelength in accordance with conservation of energy, it makes sense that all light relevant to donor and acceptor fluorescence should be transmitted, and that any light with a wavelength shorter than 550 (such as scattered laser light) will be reflected away from the optical path as seen in Figure 1.9.

Left with only the relevant signals from donor and acceptor fluorescence, from which we can ratiometrically determine FRET efficiency, a second dichroic mirror is employed to separate these signals. This mirror, a 610nm long-pass filter, reflects donor emission 90 degrees out of the optical path, to be collected by one fiber optic cable, transmitting it to an APD, while acceptor emission passes through and is

collected by another optical cable coupled to a different APD. Between the long-pass filter and each cable is a band-pass filter, centered at 575nm and 680nm for the donor and acceptor channels respectively. These function to clear away any extraneous signal and transmit only those wavelengths associated with peak donor and acceptor emission.

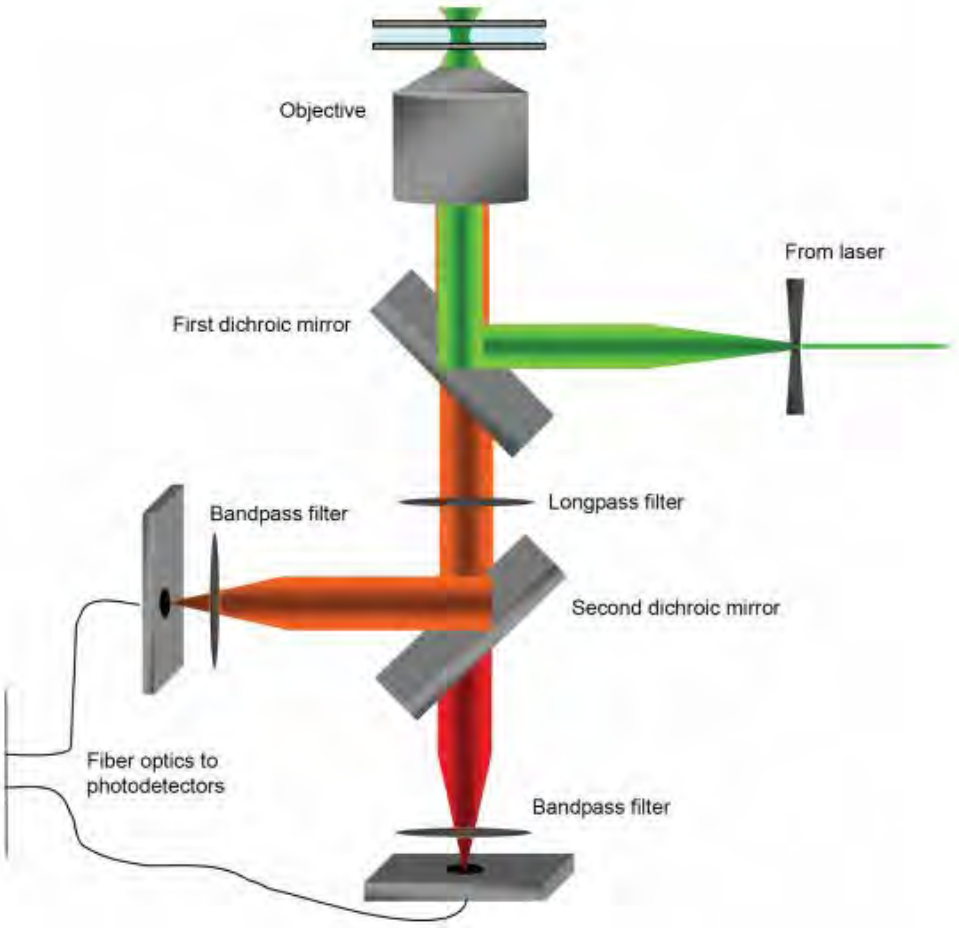

Figure 2.3: The optical path of the O'Hara lab, denoting the location of filters and mirrors as well as detectors. Adapted from ref. [66]

Although these filters are efficient in selecting for only those wavelengths with which we are concerned, there is nonetheless some donor fluorescence which will be

collected in the acceptor fluorescence channel due to the breadth of AF555's emission spectrum. This crosstalk can be experimentally determined, and correspondingly subtracted from the acceptor fluorescence channel. Alexa Fluor 647 has been previously determined to have no emission character within the range of wavelengths collected by the donor channel, and this was corroborated by our early control experiments.

ii. Experimental Procedure

This single molecule FRET apparatus described above was used for all of the data presented in this work. Previous students of the O'Hara Lab used the LabView data acquisition workspace to create code which recorded photon counts within a time bin length and total experimental time given by the user. In this work, we used a bin time of one millisecond, and a total experimental time of ten minutes. Laser power was measured at the source, and assumed a 10% loss at each mirror before entering the microscope, for a final power of approximately 1.2 mW at the rear lens of the objective.

For each trial, four samples were prepared: one containing buffer and the relevant solute only, one with only donor-labeled αBC in the buffer, one with only acceptor-labeled αBC in the buffer, and the experimental trial containing both donor- and acceptor-labeled αBC. Unless otherwise specified, each sample contained 500pM fluorescent constituents, meaning the donor- and acceptor-only samples contained 500pM total dye, and the experimental trial contained a total of 1nM dye. The first three samples in each trial were controls, and used to determine background noise and donor crosstalk during data processing. Samples were assembled from a stock of 250nM donor- and 250nM acceptor-labeled αBC stored at 4°C, with 10X buffer stock and

distilled water for dilution. Samples were diluted and assembled immediately prior to data collection.

The trials were conducted in a manner which allowed each sequential trial to be control for the next. The first trial consisted of αBC in a 100mM $NaHPO_4$, 150mM NaCl pH 7.4 buffer. This is the buffer in which the αBC was expressed and prepared, and served as a control against switching the labeled αBC into the buffer for the remaining trials, TRIS. TRIS use was necessary because of the addition of calcium in later trials, which would readily form insoluble calcium phosphate when added to a sodium phosphate solution. This would affect both the pH and salt balance of the solvent, as well as the optical clarity. The next trial was a solvent of 150mM TRIS pH 7.4. The following trial consistent of a solvent of 150mM TRIS pH 7.4 in addition to 100mM $CaCl_2$. Calcium was added in this step for several reasons. The major reason is that calcium is known to both interact directly with proteins in numerous different ways, as well modulating protein-protein interactions indirectly. Our PC source was stored in a calcium salt. By adding calcium in this step, we can parse the modulation of the FRET efficiency distribution due to calcium from that due to PC.

iii. Data Analysis

Data collected from these trials consists of three components: Bin number, which is related to time, donor channel photon count, and acceptor channel photon count. As mentioned previously, analysis of the relationship between dye diffusion times and bin length ensures that for a given bin, donor and acceptor photon counts can be attributed to the state of one pair of dye molecules. Our goal in FRET data analysis is to transform these numbers ratiometrically into a FRET efficiency, and observe the

relative frequency of each FRET efficiency to visualize a characteristic FRET distribution.

During the majority of the experimental time, there will not be a dye pair crossing the focal volume. Correspondingly, a majority of bins collected will contain only photons which can be attributed to background noise and other factors such as solution impurities or Rayleigh scattering of red-shifted excitation photons. Bins in which a dye pair crosses the focal volume are characterized by a stark increase in photon counts from the background, reflecting a series of absorption and emission events. To build a FRET efficiency distribution, we only want to use those bins which contain such fluorescence events. To segregate out these bins, we thresholded the data.

Thresholding single molecule data in the form of bins is not an exact science, and the most effective method of thresholding the data does not immediately arise from either the data or the experimental methodology. What is clear is that the thresholding criteria must retain those bins which contain a minimum number of photons so as to reflect a fluorescence event. However, there are several different ways to do this; the main three are SUM, AND, and OR criteria. SUM retains those time bins whose summed donor and acceptor channel photon counts achieve a certain number. AND selects those bins whose donor channel count is greater than some number T_D and whose acceptor channel count is greater than another number T_A. OR selects for those time bins where either the donor channel is greater than T_D or the acceptor channel count is greater than T_A. AND and OR criteria reflect inherent biases towards extreme and intermediate FRET values respectively, therefore previous analysis in the O'Hara lab was completed using a SUM criteria. However, further reflection on the use of a SUM criteria with this

particular system reveals a bias: given that the donor and acceptor dyes are on separate αBC monomers, it is not guaranteed that an acceptor dye will pass through the focal volume in a given bin. It is possible (and probable) that a lone donor dye molecule could pass through the focal volume, whose donor channel count alone could fulfill the SUM criteria. In conjunction with a low acceptor channel count attributed to background noise, this heavily biases the distribution towards low FRET values and does not accurately reflect the FRET distribution of αBC under those conditions. Since direct excitation of Alexa Fluor 647 by a 532nm excitation source is of very low likelihood, we reasoned the more selective criteria within this system is the presence of acceptor fluorescence, which can only be accomplished by FRET, guaranteeing a FRET event to be reflected by that bin. Thus, in this work we use a modified AND criteria to select for bins whose count in the acceptor channel corresponds to a fluorescence event and whose count in the donor channel is above the background signal, the determination of which will be discussed later on. It is important to acknowledge that this criteria is not prefect and possesses flaws of its own. Namely, it is possible that bins whose acceptor count is below that of the acceptor threshold do contain a fluorescence event. These low-count bins would reflect a lower FRET efficiency, and therefore one must acknowledge a bias of this criteria towards high FRET values, an explicit consequence of using the AND criteria. This can be mitigated by lowering the excitation laser power and using lower αBC concentrations, to reduce background noise and thus lower the acceptor threshold.

The selection of the value of the threshold is the next key. It must be high enough to exclude false signals due to background noise and other signal contaminants, but low

enough to include as many valid signals as possible. Although analysts have made models for selecting threshold values based on information theory, previous work of the O'Hara lab concluded that such a measure was unnecessary. Modulation of the threshold values will reveal a domain in which the distribution of FRET efficiency maxima will not shift laterally, but only vertically, reflecting a change in only frequency, rather than bias. Selecting the lowest possible value within this domain maximizes the resolution of the FRET distribution while keeping false signal inclusion low. In the process of this work, a reliable way of determining this domain was to examine the bin count frequency distribution in each channel. Low counts had the highest frequency, and the low count domain could be well-modeled by a Poisson distribution usually centered between two and four counts. This makes sense: background counts should be random variations from a mean noise value. Examining the divergence of the Poisson fit from the data at high counts revealed those most likely to be associated with fluorescence. It was determined that the lowest count at which the frequency diverged from the Poisson fit by greater than one order of magnitude reliably fulfilled the criteria of low false signal rate and horizontally stable FRET maxima, and could be used as the threshold value. In combination with criteria selection, it would be more accurate to characterize this thresholding as a FRET "fingerprint." Although it does not give the whole picture, and should be considered in the context of other clues, the precision of this data is key: the rigor with which the data is selected pushes the false signal inclusion rate to vanishingly small when compared to other methodologies. This is at the expense of a more complete distribution.

Once the data has been thresholded, a FRET efficiency can be calculated for each bin. As discussed in Section I, the FRET efficiency value is given by

$$E = \frac{I_A}{I_A + I_D},$$

where E is the efficiency and I_A and I_D are the acceptor and donor signal intensities (reported by photon counts in this work) respectively. However, using the raw photon counts recorded in the data would include background noise and crosstalk between the channels. Therefore, it is more accurate to report the efficiency value as

$$E = \frac{I_A - B_A - C_A I_A}{(I_A - B_A - C_A I_A) + (I_D - B_D - C_D I_D)},$$

where B and $C*I$ denote the portion of the signal due to background noise and channel crosstalk respectively. The background signal for each channel was taken as the average signal in that channel in the buffer-only sample within a given trial. It is worth noting that despite using ostensibly the same laser power, previous work of the O'Hara lab reported background values less than or equal to 1, while the majority of trials in this work contained background signal values of between 2 and 3. After thresholding the donor- and acceptor-labeled control samples in the manner described above, channel crosstalk was calculated. C_A was determined by dividing the average donor fluorescence by the average acceptor fluorescence in the acceptor-labeled control sample, and C_D by dividing the average acceptor fluorescence signal by the average donor fluorescence signal in the donor-labeled control sample. After data underwent this background and crosstalk correction, we assembled FRET efficiency distribution histograms.

III. Results

A. Sodium Phosphate

The first trial of the series was 500pM AF555-labeled αBC with 500pM AF647-labeled αBC in 150mM monobasic sodium phosphate buffer at pH 7.4. This trial served as a form of calibration of the system. Previous work of the O'Hara lab had confirmed that the set-up was able to measure FRET in αBC systems, although particular observation of S85C mutants with these dyes had not been completed before. As such, we postulated that αBC in this particular buffer and pH was a baseline distribution, to which we can compare subsequent trials. Some prediction can be made as to an expected FRET distribution based on models of αBC oligomers, by taking theoretical structures such as 3J07, measure all of the inter-dye distances, converting them to efficiencies, and placing them in the FRET distribution. This proved to be time intensive, and such an analysis did not seem necessary in work regarding a relative change in distribution, as opposed to work dealing in absolute frequencies.

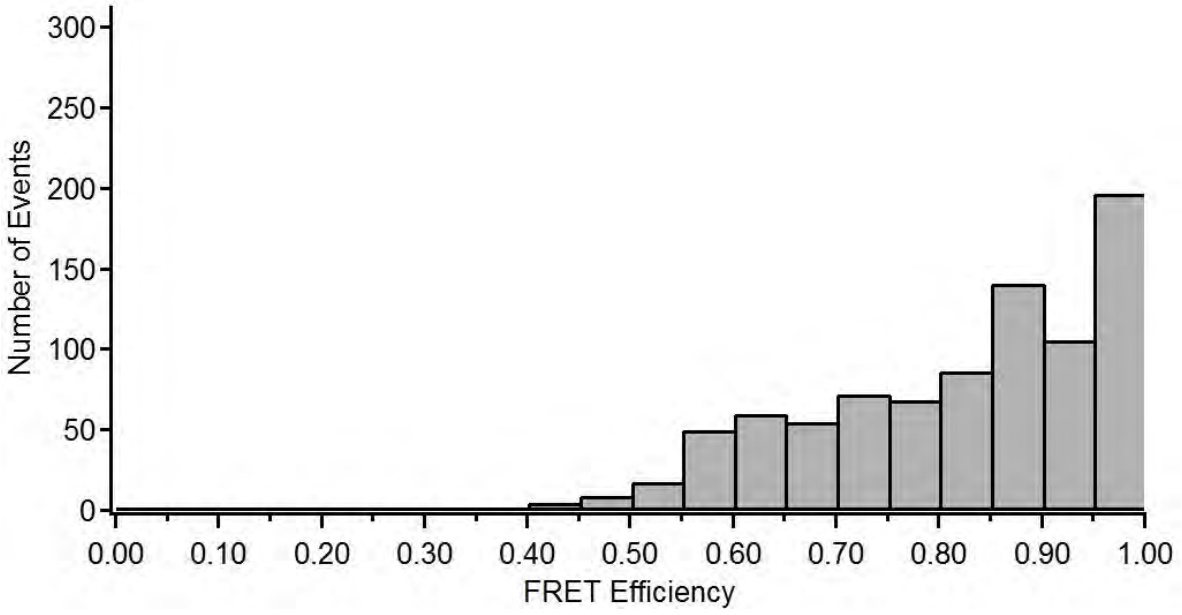

Figure 3.1: FRET distribution of 500pM AF555-labeled αBC with 500pM AF647-labeled αBC in 150mM monobasic sodium phosphate buffer at pH 7.4. Data from *n=6* trials averaged to give frequencies reflecting 10 minutes of collection.

These results are not what one would consider a 'typical' FRET distribution. Even taking into account the inherent biases in thresholding explained in the previous chapter, one would still expect to see some population of low efficiency FRET values. Nonetheless, this previously dubbed FRET "fingerprint" is all we need to accurately qualify changes in oligomeric distribution. This is because all the theoretical efficiencies extracted from structural models denoting inter-dye distances are within the range of .5 to .95. This assumes that oligomeric species can be semi-uniquely identified by their inter-dye distances and corresponding frequencies. Two measures were taken to try and lower this threshold: lower laser power and lower concentrations of αBC. However, 1nM total protein concentration and 2.0mW source power were the lowest parameters at which the distribution was consistent. This is opposed to previous work of the O'Hara lab and most single-molecule work cited here, which generally used total protein concentrations on the order of 100nM.

B. TRIS-Base

The second trial was conducted with the same protein concentrations, this time in 150mM TRIS-Base pH balanced to 7.4. As previously mentioned, this trial serves as a control against the subsequent trials containing Ca(II) from calcium chloride. This calcium would precipitate out in the form of calcium phosphate if it were to be added to the storage buffer of sodium phosphate. As such, a buffer switch from sodium phosphate to TRIS-Base, which does not precipitate Ca(II), was necessary. We expected

that this trial would reveal a FRET distribution identical to that of sodium phosphate, as we did not expect that the buffer would have a significant effect.

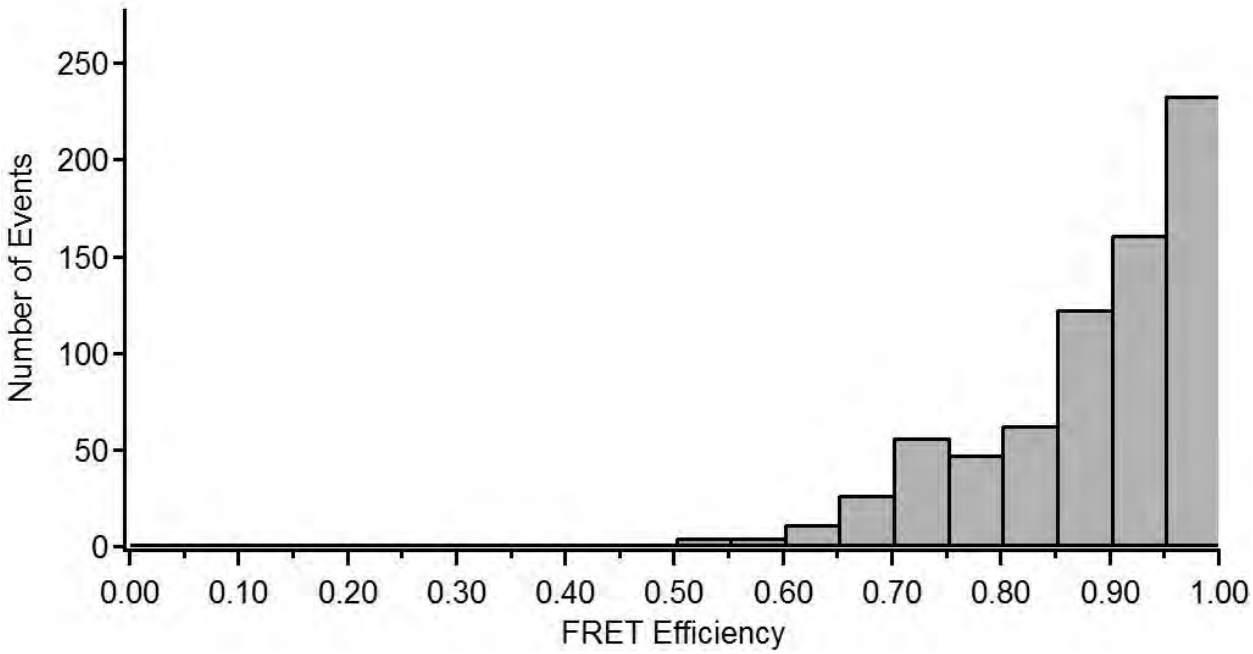

Figure 3.2: FRET distribution of 500pM AF555-labeled αBC with 500pM AF647-labeled αBC in 150mM TRIS-Base at pH 7.4. Data from *n=4* trials averaged to give frequencies reflecting 10minutes of collection.

In accord with our expectations, the FRET distributions of sodium phosphate and TRIS-Base are very similar. There is a noticeable difference in shape at low FRET efficiency, but we do not believe this to reflect a significant real change in the oligomeric distribution of αBC. If it were to reflect a change, it makes sense that the larger oligomers of αBC--which are the source of lower efficiency signals according to recent oligomeric models--would be most susceptible to small perturbations like a buffer change.

C. TRIS-Base and Calcium Chloride

The next trial tested the role of Ca(II) in αBC oligomerization. The solvent consisted of 150mM TRIS-Base and 100mM calcium chloride with the usual total protein concentration of 1nM pH balanced to 7.4. Admittedly, such an incredibly high concentration of calcium does not reflect intracellular conditions, even in cortical cataracts, which display significantly increased calcium concentrations. Normal eye lens calcium concentrations are reported to be in the .1-1mM range, while cataractous lens have been reported to contain up to 50mM calcium in the upper bound. Our reasons for performing these experiments in these extreme conditions are two-fold: the PC used in subsequent trials was stored as a calcium salt, thus closely matching the resultant concentration of calcium in solutions containing PC provided an easy way to parse FRET distribution modulation due to calcium from that due to PC without introducing dialysis or other methods of ion concentration change; and subunit exchange kinetics are not reported to be affected by calcium concentrations of up to 50mM (the maximum concentration used in the study).

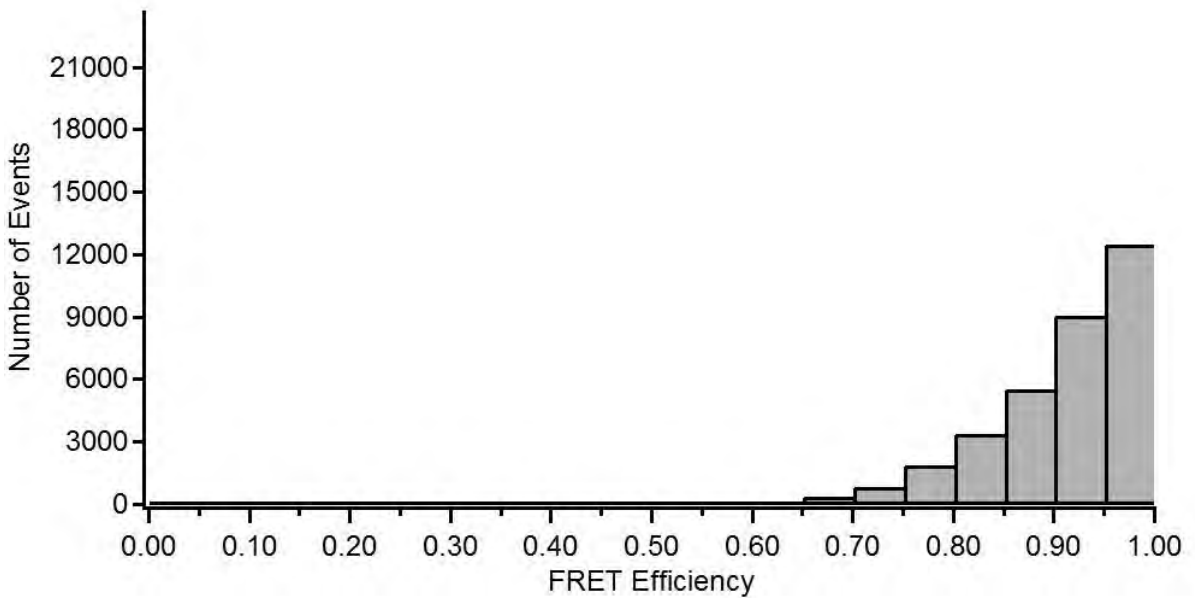

Figure 3.3: FRET distribution of 500pM AF555-labeled αBC with 500pM AF647-labeled αBC in 150mM TRIS-Base and 100mM calcium chloride at pH 7.4. Data from *n=3* trials averaged to give frequencies reflecting 10minutes of collection.

Our initial results did not make much sense. Based on previous studies of calcium-induced αBC functional and structural modification, we did not expect to see a 100-fold increase in the number of bins containing a FRET event, nor did we expect to see such a large change in the shape of the FRET distribution. However, there are several reasons supporting these results as reflective of a physical change within the sample.

The most obvious reason is the consistency in overall FRET bins. Over the course of several days containing several trials, the number of bins meeting the FRET criteria stayed within the same order of magnitude. Previous trials of sodium phosphate and TRIS displayed a similar degree of consistency. In addition, the overall photon count

was consistent not only between days, but was consistent with sodium phosphate and TRIS trials. That is, the sum of all photons collected during the experiment between the two channels was on the same order of magnitude consistently, the major change being an approximately nine-fold increase in the total number of acceptor photons and a five-fold reduction in the number of donor photons (the donor channel consistently collected more photons over all trials, which makes sense). Further, if the drastic increase in acceptor photon counts was due to scattering events, we would expect to see not just a similar uptick in the donor channel, but a greater increase. This is because the intensity of light due to scattering is proportional to $\frac{1}{\lambda^4}$, where λ is the wavelength of the incident light. Therefore the donor channel, which records wavelengths smaller than that of the acceptor channel, should record more scattered light. This was not the case. The major deterrent from interpreting this data as reflective of the system came from its distribution variance. Although the total FRET bin count and total photon count stayed consistent, the shape of the distribution did not. As such, we are not confident that this major difference in the data can be attributed to an actual change in the system.

Even though these results were not consistent with scattering effects, we deemed filtering the sample solution an easy way to test this. Instead of preparing a usual sample volume of 200μL, a total sample volume of 3mL was made, and filtered through a .22μm syringe filter, from which a 200μL sample volume was taken. The resultant FRET distribution was very similar to that of sodium phosphate and TRIS-based solvents. Despite evidence to the contrary, these results clearly indicate the presence of aggregate species larger than 220nm, consistent with sizes which would

scatter light and produce an inconsistent FRET distribution. Filtered solutions did display slightly lower total photon counts during the FRET assay, but stayed within an order of magnitude of total photon counts from previous solvents. This makes sense, should the filtered aggregates contain some amount of αBC.

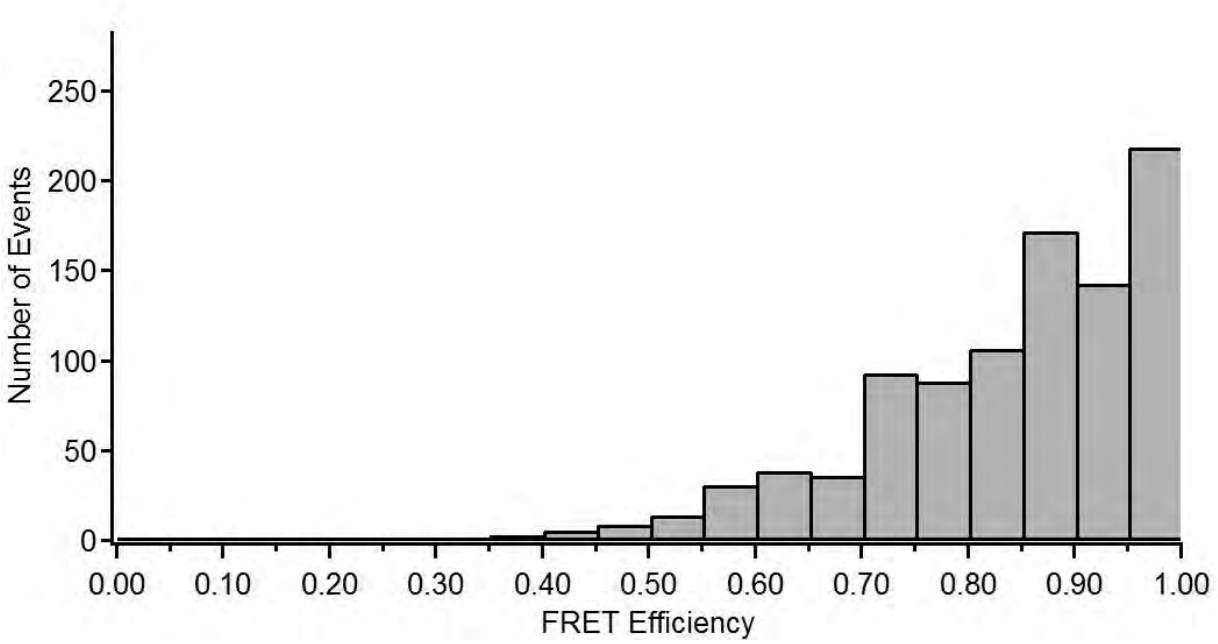

Figure 3.4: FRET distribution of 500pM AF555-labeled αBC with 500pM AF647-labeled αBC in 150mM TRIS-Base and 100mM calcium chloride at pH 7.4 filtered through a .22μm syringe filter. Data from *n=7* trials averaged to give frequencies reflecting 10minutes of collection.

D. Phosphocholine and Calcium Chloride

The last trial consisted of 150mM PC, whose calcium chloride storage salt added 150mM calcium chloride. PC can act as its own buffer, with a secondary phosphate pK_a of approximately 8.0, retaining significant buffering capacity when balanced to pH 7.4.

Results were very similar to those of the TRIS and calcium chloride solvent, including aberrant FRET distributions when unfiltered.

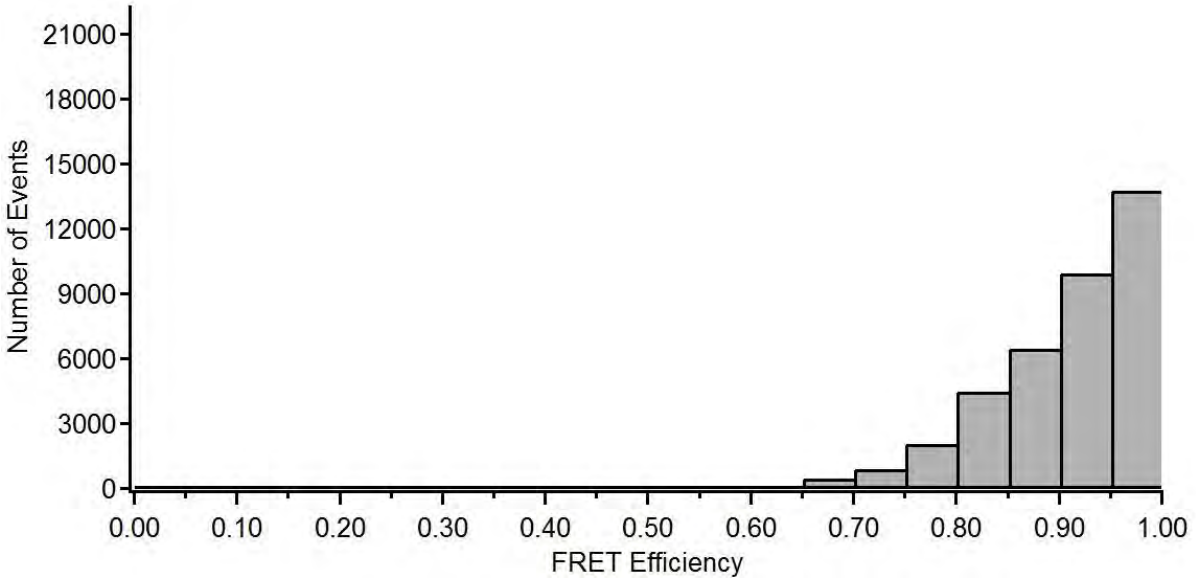

Figure 3.5: FRET distribution of 500pM AF555-labeled αBC with 500pM AF647-labeled αBC in 150mM PC and 150mM calcium chloride at pH 7.4. Data from *n=3* trials averaged to give frequencies reflecting 10minutes of collection.

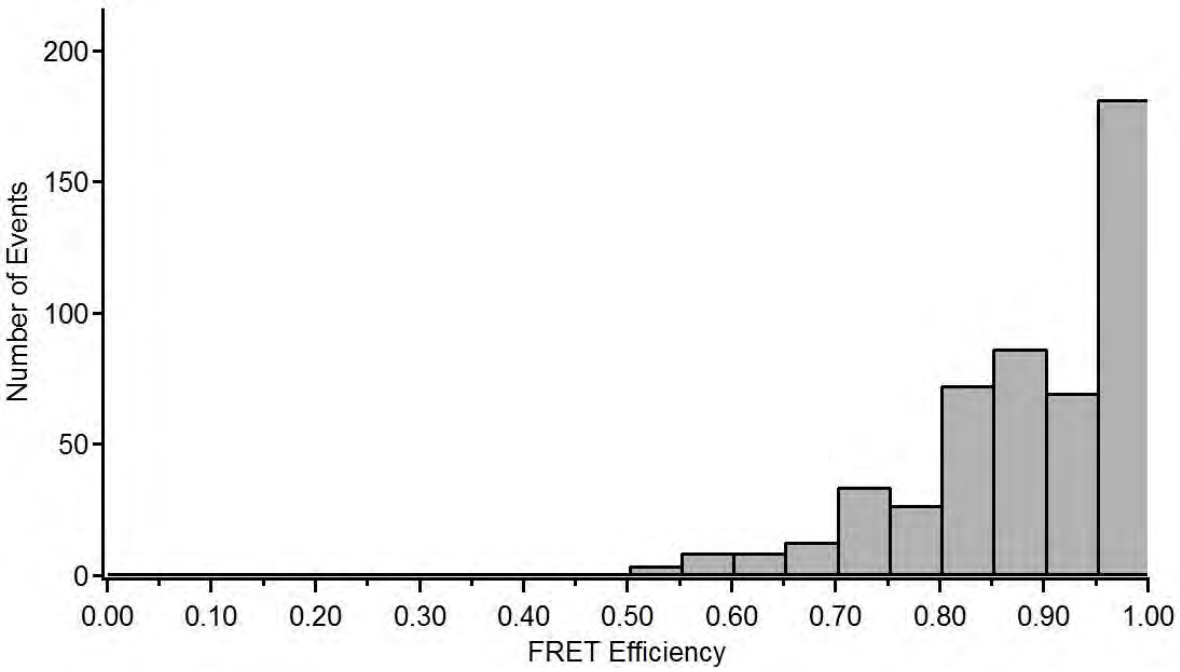

Figure 3.6: FRET distribution of 500pM AF555-labeled αBC with 500pM AF647-labeled αBC in 150mM PC and 150mM calcium chloride at pH 7.4 filtered through a .22μm syringe tip filter. Data from *n=4* trials averaged to give frequencies reflecting 10minutes of collection.

IV. Discussion

In this work we sought to investigate the role of calcium and PC in αBC oligomerization, and whether or not their role could be related to their respective experimentally observed quantities and locations. Considering the results of our single molecule FRET analysis, our work evidences little to no interaction of calcium and PC with αBC, and no apparent modulation of αBC oligomerization. This is based on the assumption that the phenomenon observed in unfiltered solutions containing calcium was not indicative of a change in oligomerization of αBC or reflective of a change in the tertiary structure of αBC itself, because the frequency and shape of the FRET distribution did not change once filtered. If a significant portion of αBC was aggregating, we would expect to see a corresponding significant reduction in FRET frequency and a reduction in the overall number of photons collected. This was evidently not the case. A definitive answer as to whether or not this is the case is outside the scope of this work, both temporally and methodologically.

With respect to calcium, our results are inconclusive. On one hand, it is not surprising that it had little effect. Previous studies have shown crystallins to have a robust resistance to cation interference, both in structure and in function. Intuitively this makes sense--once it has been established that crystallin folding does not heavily rely on electrostatic interactions, introducing ions into the solution should not strongly affect their structure. On the other hand, it is surprising that there was little modulation, given the extreme conditions. It has been shown that αBC aggregates at concentrations of calcium much lower than what we used, so there remains a question as to how our αBC resisted aggregation, and the degree to which it actually resisted. Possible explanations include the exceedingly low protein concentrations necessary for single

molecule assays preventing one molecule from finding the next, as well as the slightly basic pH at which trials were conducted, which Hightower et al. reported to be effective at inhibiting aggregation.

With respect to PC, our results are less surprising. The theory of αBC's general mechanism relies on exposed hydrophobic surfaces, of which PC realistically has none. It is far more likely that αBC prefers to associate with hydrophobic surfaces briefly exposed to solvent, and thus αBC's affinity for nuclear cell membranes is better explained by the changing behavior and fluidity of the membrane rather than the constituency of the lipid headgroups. Nonetheless, these results are helpful in narrowing the scope of an explanation for αBC's membrane affinity.

Bibliography

1. Anfinsen, C. B. Principles that Govern the Folding of Protein Chains. *Science* **181,** 223–230 (1973).
2. Kubelka, J., Hofrichter, J. & Eaton, W. A. The protein folding 'speed limit'. *Curr. Opin. Struct. Biol.* **14,** 76–88 (2004).
3. Hartl, F. U., Bracher, A. & Hayer-Hartl, M. Molecular chaperones in protein folding and proteostasis. *Nature* **475,** 324–332 (2011).
4. Haslbeck, M. & Vierling, E. A First Line of Stress Defense: Small Heat Shock Proteins and Their Function in Protein Homeostasis. *J. Mol. Biol.* **427,** 1537–1548 (2015).
5. Ritossa, F. A new puffing pattern induced by temperature shock and DNP in drosophila. *Experientia* **18,** 571–573 (1962).
6. Tissiéres, A., Mitchell, H. K. & Tracy, U. M. Protein synthesis in salivary glands of Drosophila melanogaster: Relation to chromosome puffs. *J. Mol. Biol.* **84,** 389–398 (1974).
7. Georgopoulos, C. P., Hendrix, R. W., Casjens, S. R. & Kaiser, A. D. Host participation in bacteriophage lambda head assembly. *J. Mol. Biol.* **76,** 45–60 (1973).
8. Sternberg, N. Properties of a mutant of Escherichia coli defective in bacteriophage lambda head formation (groE). II. The propagation of phage lambda. *J. Mol. Biol.* **76,** 25–44 (1973).

9. Goloubinoff, P., Gatenby, A. A. & Lorimer, G. H. GroE heat-shock proteins promote assembly of foreign prokaryotic ribulose bisphosphate carboxylase oligomers in Escherichia coli. *Nature* **337,** 44–47 (1989).
10. Hightower, L. E. Heat shock, stress proteins, chaperones, and proteotoxicity. *Cell* **66,** 191–197 (1991).
11. Chiti, F. & Dobson, C. M. Protein misfolding, functional amyloid, and human disease. *Annu. Rev. Biochem.* **75,** 333–366 (2006).
12. Renkawek, K., Voorter, C. E., Bosman, G. J., van Workum, F. P. & de Jong, W. W. Expression of alpha B-crystallin in Alzheimer's disease. *Acta Neuropathol. (Berl.)* **87,** 155–160 (1994).
13. Sun, Y. & MacRae, T. H. The small heat shock proteins and their role in human disease. *FEBS J.* **272,** 2613–2627 (2005).
14. van Noort, J. M. *et al.* The small heat-shock protein αB-crystallin as candidate autoantigen in multiple sclerosis. *Nature* **375,** 798–801 (1995).
15. Horwitz, J. Alpha-crystallin can function as a molecular chaperone. *Proc. Natl. Acad. Sci. U. S. A.* **89,** 10449–10453 (1992).
16. Basha, E. *et al.* The Identity of Proteins Associated with a Small Heat Shock Protein during Heat Stress in Vivo Indicates That These Chaperones Protect a Wide Range of Cellular Functions. *J. Biol. Chem.* **279,** 7566–7575 (2004).
17. Mainz, A. *et al.* The chaperone αB-crystallin uses different interfaces to capture an amorphous and an amyloid client. *Nat. Struct. Mol. Biol.* **22,** 898–905 (2015).
18. Basha, E., O'Neill, H. & Vierling, E. Small heat shock proteins and α-crystallins: dynamic proteins with flexible functions. *Trends Biochem. Sci.* **37,** 106–117 (2012).

19. Mchaourab, H. S., Godar, J. A. & Stewart, P. L. Structure and mechanism of protein stability sensors: The chaperone activity of small heat-shock proteins. *Biochemistry (Mosc.)* **48,** 3828–3837 (2009).
20. Hu, W.-F. *et al.* αA- and αB-crystallins interact with caspase-3 and Bax to guard mouse lens development. *Curr. Mol. Med.* **12,** 177–187 (2012).
21. Hilton, G. R., Lioe, H., Stengel, F., Baldwin, A. J. & Benesch, J. L. P. Small heat-shock proteins: paramedics of the cell. *Top. Curr. Chem.* **328,** 69–98 (2013).
22. Jakob, U. & Buchner, J. Assisting spontaneity: the role of Hsp90 and small Hsps as molecular chaperones. *Trends Biochem. Sci.* **19,** 205–211 (1994).
23. Lee, G. J., Roseman, A. M., Saibil, H. R. & Vierling, E. A small heat shock protein stably binds heat-denatured model substrates and can maintain a substrate in a folding-competent state. *EMBO J.* **16,** 659–671 (1997).
24. Engelsman, J. den, Keijsers, V., Jong, W. W. de & Boelens, W. C. The Small Heat-shock Protein αB-Crystallin Promotes FBX4-dependent Ubiquitination. *J. Biol. Chem.* **278,** 4699–4704 (2003).
25. Goldman, J. E. & Corbin, E. Rosenthal fibers contain ubiquitinated alpha B-crystallin. *Am. J. Pathol.* **139,** 933–938 (1991).
26. Gopalakrishnan, S. & Takemoto, L. Binding of actin to lens alpha crystallins. *Curr. Eye Res.* **11,** 929–933 (1992).
27. Wang, K. & Spector, A. alpha-crystallin stabilizes actin filaments and prevents cytochalasin-induced depolymerization in a phosphorylation-dependent manner. *Eur. J. Biochem.* **242,** 56–66 (1996).

28. Ghosh, J. G., Houck, S. A. & Clark, J. I. Interactive Domains in the Molecular Chaperone Human αB Crystallin Modulate Microtubule Assembly and Disassembly. *PLOS ONE* **2,** e498 (2007).

29. Xi, J.-H., Bai, F., McGaha, R. & Andley, U. P. Alpha-crystallin expression affects microtubule assembly and prevents their aggregation. *FASEB J. Off. Publ. Fed. Am. Soc. Exp. Biol.* **20,** 846–857 (2006).

30. Nicholl, I. D. & Quinlan, R. A. Chaperone activity of alpha-crystallins modulates intermediate filament assembly. *EMBO J.* **13,** 945–953 (1994).

31. Miesbauer, L. R. *et al.* Post-translational modifications of water-soluble human lens crystallins from young adults. *J. Biol. Chem.* **269,** 12494–12502 (1994).

32. Smith, J. B., Sun, Y., Smith, D. L. & Green, B. Identification of the posttranslational modifications of bovine lens alpha B-crystallins by mass spectrometry. *Protein Sci. Publ. Protein Soc.* **1,** 601–608 (1992).

33. Ito, H., Okamoto, K., Nakayama, H., Isobe, T. & Kato, K. Phosphorylation of αB-Crystallin in Response to Various Types of Stress. *J. Biol. Chem.* **272,** 29934–29941 (1997).

34. Bakthisaran, R., Akula, K. K., Tangirala, R. & Rao, C. M. Phosphorylation of αB-crystallin: Role in stress, aging and patho-physiological conditions. *Biochim. Biophys. Acta BBA - Gen. Subj.* **1860,** 167–182 (2016).

35. Labbadia, J. & Morimoto, R. I. The Biology of Proteostasis in Aging and Disease. *Annu. Rev. Biochem.* **84,** 435–464 (2015).

36. Brady, J. P. *et al.* Targeted disruption of the mouse αA-crystallin gene induces cataract and cytoplasmic inclusion bodies containing the small heat shock protein αB-crystallin. *Proc. Natl. Acad. Sci. U. S. A.* **94,** 884–889 (1997).
37. Boyle, D. L., Takemoto, L., Brady, J. P. & Wawrousek, E. F. Morphological characterization of the Alpha A- and Alpha B-crystallin double knockout mouse lens. *BMC Ophthalmol.* **3,** 3 (2003).
38. Delaye, M. & Tardieu, A. Short-range order of crystallin proteins accounts for eye lens transparency. *Nature* **302,** 415–417 (1983).
39. Horwitz, J., Bova, M. P., Ding, L.-L., Haley, D. A. & Stewart, P. L. Lens α-crystallin: Function and structure. *Eye* **13,** 403–408 (1999).
40. Kasthurirangan, S., Markwell, E. L., Atchison, D. A. & Pope, J. M. In vivo study of changes in refractive index distribution in the human crystalline lens with age and accommodation. *Invest. Ophthalmol. Vis. Sci.* **49,** 2531–2540 (2008).
41. Kriehuber, T. *et al.* Independent evolution of the core domain and its flanking sequences in small heat shock proteins. *FASEB J. Off. Publ. Fed. Am. Soc. Exp. Biol.* **24,** 3633–3642 (2010).
42. Poulain, P., Gelly, J.-C. & Flatters, D. Detection and Architecture of Small Heat Shock Protein Monomers. *PLOS ONE* **5,** e9990 (2010).
43. Ghosh, J. G. & Clark, J. I. Insights into the domains required for dimerization and assembly of human αB crystallin. *Protein Sci. Publ. Protein Soc.* **14,** 684–695 (2005).
44. Horwitz, J. Alpha-Crystallin: The Quest For A Homogeneous Quaternary Structure. *Exp. Eye Res.* **88,** 190–194 (2009).

45. Bagnéris, C. *et al.* Crystal Structures of α-Crystallin Domain Dimers of αB-Crystallin and Hsp20. *J. Mol. Biol.* **392,** 1242–1252 (2009).
46. Laganowsky, A. *et al.* Crystal structures of truncated alphaA and alphaB crystallins reveal structural mechanisms of polydispersity important for eye lens function. *Protein Sci. Publ. Protein Soc.* **19,** 1031–1043 (2010).
47. Jehle, S. *et al.* Solid-state NMR and SAXS studies provide a structural basis for the activation of αB-crystallin oligomers. *Nat. Struct. Mol. Biol.* **17,** 1037–1042 (2010).
48. Pasta, S. Y., Raman, B., Ramakrishna, T. & Rao, C. M. The IXI/V motif in the C-terminal extension of alpha-crystallins: alternative interactions and oligomeric assemblies. *Mol. Vis.* **10,** 655–662 (2004).
49. Clark, J. I. Functional sequences in human alphaB crystallin. *Biochim. Biophys. Acta BBA - Gen. Subj.* **1860,** 240–245 (2016).
50. Kundu, M., Sen, P. C. & Das, K. P. Structure, stability, and chaperone function of alphaA-crystallin: role of N-terminal region. *Biopolymers* **86,** 177–192 (2007).
51. Pasta, S. Y., Raman, B., Ramakrishna, T. & Rao, C. M. Role of the conserved SRLFDQFFG region of alpha-crystallin, a small heat shock protein. Effect on oligomeric size, subunit exchange, and chaperone-like activity. *J. Biol. Chem.* **278,** 51159–51166 (2003).
52. Aquilina, J. A., Benesch, J. L. P., Bateman, O. A., Slingsby, C. & Robinson, C. V. Polydispersity of a mammalian chaperone: Mass spectrometry reveals the population of oligomers in αB-crystallin. *Proc. Natl. Acad. Sci. U. S. A.* **100,** 10611–10616 (2003).

53. Aquilina, J. A., Shrestha, S., Morris, A. M. & Ecroyd, H. Structural and functional aspects of hetero-oligomers formed by the small heat shock proteins αB-crystallin and HSP27. *J. Biol. Chem.* **288,** 13602–13609 (2013).

54. Baldwin, A. J., Lioe, H., Robinson, C. V., Kay, L. E. & Benesch, J. L. P. αB-Crystallin Polydispersity Is a Consequence of Unbiased Quaternary Dynamics. *J. Mol. Biol.* **413,** 297–309 (2011).

55. Peschek, J. *et al.* Regulated structural transitions unleash the chaperone activity of αB-crystallin. *Proc. Natl. Acad. Sci. U. S. A.* **110,** E3780–E3789 (2013).

56. Jehle, S. *et al.* N-terminal domain of αB-crystallin provides a conformational switch for multimerization and structural heterogeneity. *Proc. Natl. Acad. Sci. U. S. A.* **108,** 6409–6414 (2011).

57. Delbecq, S. P. & Klevit, R. E. One size doesn't fit all: the oligomeric states of αB crystallin. *FEBS Lett.* **587,** (2013).

58. Hightower, K. R. Cytotoxic effects of internal calcium on lens physiology: a review. *Curr. Eye Res.* **4,** 453–459 (1985).

59. Borchman, D. & Yappert, M. C. Lipids and the ocular lens. *J. Lipid Res.* **51,** 2473–2488 (2010).

60. Jedziniak, J. A., Kinoshita, J. H., Yates, E. M., Hocker, L. O. & Benedek, G. B. Calcium-Induced Aggregation of Bovine Lens Alpha Crystallins. *Invest. Ophthalmol. Vis. Sci.* **11,** 905–915 (1972).

61. Hightower, K. R., McCready, J. P. & Goudsmit, E. M. Calcium-induced opacification is dependent upon lens pH. *Curr. Eye Res.* **6,** 1415–1420 (1987).

62. Nikbakht, M. R., Ashrafi-Kooshk, M. R., Jaafari, M., Ghasemi, M. & Khodarahmi, R. Does Long-Term Administration of a Beta-Blocker (Timolol) Induce Fibril-Based Cataract Formation In-vivo? *Iran. J. Pharm. Res. IJPR* **13,** 599–612 (2014).
63. Cobb, B. A. & Petrash, J. M. α-Crystallin Chaperone-like Activity and Membrane Binding in Age-Related Cataracts. *Biochemistry (Mosc.)* **41,** 483–490 (2002).
64. Diwan, J. Lipids and Membrane Structure.
65. So, P. T. & Dong, C. Y. Fluorescence spectrophotometry. *eLS* (2002).
66. Helinski, G. Probing the conformational distribution of the T7-RNA polymerase promoter DNA sequence using single molecule fluorescence spectroscopy. (Amherst College, 2004).
67. Pearlman, A. Characterizing the Role of C-Terminal Strand Exchange in AlphaB-Crystallin Oligomerization. (Amherst College, 2013).